Hindawi
Advances in Civil Engineering
Volume 2024, Article ID 6644300, 13 pages
https://doi.org/10.1155/2024/6644300

Research Article

Experimental Study on Consolidation Characteristics of Concentrated Full Tailings and Research on Pore Water Relief Methods of Piles

Sha Wang[1,2] **Guodong Mei**[1,2] **Yifan Chu**[1,2] **Weixiang Wang**[1,2] **Yali Wang**[1,2] **and Lijie Guo**[1,2]

[1]*BGRIMM Technology Group, No. 22, Beixing Road, Daxing District, Beijing 102628, China*
[2]*National Centre for International Research on Green Metal Mining, No. 22, Beixing Road, Daxing District, Beijing 102628, China*

Correspondence should be addressed to Guodong Mei; meiguodong@bgrimm.com and Lijie Guo; guolijie@bgrimm.com

Received 21 November 2023; Revised 11 March 2024; Accepted 8 April 2024; Published 29 April 2024

Academic Editor: Adolfo Preciado

Surface harmless storage of concentrated full tailings (CFTs) involves the technology of adding a curing agent to the tailings slurry discharged from the thickener to realize the modification of the tailings and centralized storage of the tailings on the surface to realize the harmless treatment of the tailings. High water content of tailings is still the key technical problem that restricts the harmless storage of piles at present. Regarding the above problems, we implemented the consolidation test and numerical simulation of seepage-stress coupling consolidation of CFT, clarified the consolidation characteristics and parameters of CFT under different curing ages, and conducted a comparative analysis of pore water pressure in the whole cross-section of piles with different drainage schemes based on the results of the test. In addition, we also clarified the drainage effect of interlayer drainage on reducing the excess pore water pressure of piles and compared the simulation results of the pore water pressure of piles under different permeability coefficients. The results show that as the permeability coefficient of the concentrated tailings material decreases, the pore pressure accumulation inside piles under the same drainage scheme is more serious, and the length of time for consolidation and stabilization becomes longer. Therefore, it is recommended that the excess porous water pressure be relieved by means of increased drainage facilities under a small permeability coefficient.

1. Introduction

Tailings arise as wastes are generated by the metal ore sorting process. In a traditional disposal method, they are always stored in preconstructed tailing ponds to minimize the environmental hazards. Over the years, tailings ponds have played an important role in preventing proliferation, centralizing management, and reducing risk. However, due to the huge scale of the tailings pond site, the risk of rainfall scouring and transferring, and the risk of water catchment in the pond leading to instantaneous collapse of the dam crest and uplift of the seepage line, accidents such as tailings leakage and tailings pond collapse have occurred over the years, which have resulted in huge safety and environmental problems. Therefore, the harmless disposal of tailings is a key technical problem that needs to be solved urgently.

CFT surface harmless storage technology is to add a high efficient curing agent to tailings to reduce the migration rate of harmful substances in tailings and design a unique storage section to realize the surface stacking of tailings. The curing agent and the special design section can improve the strength of the tailings pile and enhance the scour resistance of the pile and the overall antislip stability. The material ratio of CFT is somewhat similar to that of the underground tailings cemented filler. However, there are major differences in the surface water and air working conditions and the storage environment, and it is necessary to carry out a special study on the mechanical properties of CFT for the surface environment. During surface harmless storage, the volume ratio of tailings material volume to water can reach 1 : 1, indicating a high water content. The hydration reaction of cement, flyash, and other cementitious materials contained in the curing

agent has certain requirements on the upper limit of water content, so the efficient relief of water is not only related to the results of the effective stress in the pile project but also affects the final effect of the hydration reaction of the cementitious materials [1, 2], thus affecting the mechanical strength of the tailings consolidated materials [3, 4]. Given this, the main contradiction in the surface harmless storage of CFT is focused on the efficient method of excess water relief, and how to solve the relief problem of excess pore water pressure in the process of storage is the key technical problem related to the success or failure of the storage.

Since curing conditions are important factors affecting the consolidation characteristics of tailings materials. Xu et al. [5], Chen et al. [6], Benkirane [7], Fan et al. [8], Yilmaz et al. [9], Qin et al. [10], Li [11], Ke [12], and Deng et al. [13] carried out an experimental study on the consolidation characteristics of tailings cements with different curing conditions (different age, temperature, humidity, stress, etc.). They identified the main factors and critical conditions affecting the consolidation of tailings binder. It was clarified that a good curing conditions at the early stage is the most effective means to ensure the strength of tailings binder and influence its final consolidation effect [14–16]. Ma et al. [17] conducted a study on the effect of drainage conditions on the consolidation characteristics of tailings slurry in a filled quarry, pointing out that the effectiveness of drainage during the accumulation process is the main factor affecting the consolidation characteristics of tailings slurry. In addition to the study of the effect of curing conditions on the consolidation of tailings slurry, the optimization of the material ratio is also a major research direction to improve the consolidation strength of tailings slurry. For example, adding fibers [18–20] to the tailings slurry, or using fine tailings slurry [21], or using different curing cements or admixtures [22, 23], etc., in order to improve the final mechanical properties of the tailings solidification body by changing the mix proportion of each material. Nonetheless, the study results showed that in the case of high water content, there is a minor effect of improving the final strength of tailings slurry by ratio optimization.

Indoor tests are conducted under ideal conditions, and the strength growth pattern in outdoor environments, especially under extreme environmental conditions, will deviate from the ideal state. Wang et al. [24] carried out an experimental study on the consolidation characteristics of tailings cemented filler in Alpine regions, and Hou et al. [25] launched a study on the effect of freeze–thaw cycles on the strength of full tailings consolidation and obtained the growth pattern of the strength of tailings cemented consolidation at extreme temperatures. Under the cold condition, the excess free water will make the tailings cement produce the freezing and thawing effect if the free water is not removed in time, which will change the hydration reaction process and have a more unfavorable effect on the strength of the tailings cement. The problem of free water removal is more urgent than that of the normal air temperature condition.

Due to the huge volume of the concentrated tailings pile, and with the layer by layer paving method in the construction process, the materials in the lower part of the pile are constantly subjected to the self-weight of the upper part of the cyclic loading, and the consolidation of the concentrated tailings cement takes place over a long period of time. In this process, the water body is constantly drained, the pore space is continuously compacted, and the hydration reaction results in a gradual increase in the strength of the concentrated tailings cement with time. Consequently, there is great importance in studying the long-term mechanical behavior of tailings cements, such as the study of consolidation behavior under cyclic loading [26] and creep characteristics and long-term strength [27, 28] study. Wang et al. [29] carried out dynamic triaxial tests to study the consolidation and reconsolidation characteristics of tailings and proposed the relationship between the ratio of the cycle number of liquefaction after reconsolidation to the cycle number of first liquefaction and the reconsolidation degree. In order to study the shear wave velocity (Vs) of unsaturated tailings, Cao et al. [30] carried out triaxial tests with different effective stresses and void ratios, the test results showed that the soil water characteristic curve of the unsaturated tailing soils is similar to that of other sandy soils, and Vs is strongly related to effective stress, grain size, and void ratio. Furthermore, due to the large scale of the field stockpile, which is not suitable for the use of the basic assumption of small deformation, Ito and Azam [31] conducted a consolidation analysis of the tailings cements by using the theory of large deformation. Meanwhile, given the complex seepage–mechanical field coupling during the consolidation process, Cui and Fall [32] proposed a multiphysics model for calculating the consolidation displacement of the tailings cement. Shahsavari and Grabinsky [33] investigated the change rule of pore water pressure during the filling process of consolidated tailings, and Erçikdi et al. [34] studied the effect of drainage conditions on the growth of strength of consolidated tailings, and the results showed that favorable drainage conditions are favorable for the growth of strength of consolidated tailings.

The curing environment for the surface harmless storage of CFT is quite different from that of underground filling, and the ratio design of consolidated tailings is different from that of underground filling materials. For this reason, special studies are needed on the consolidation characteristics of CFT and the drainage mode of the piles, in order to clarify the changing law of the consolidation characteristics of CFT, to determine the drainage scheme of the piles, and to guide the sectional design and structural design of the CFT piles.

Accordingly, the technical route to be adopted in this study is demonstrated graphically in Figure 1, i.e., adopting solidification test, numerical simulation, comparative analysis, and other methods to obtain the change rule of porosity and displacement of the concentrated tailings under different loads. On this basis, we performed numerical simulation analysis of consolidation, and coupled stress–seepage field calculations based on the initial porosity and permeability coefficient and other parameter settings. After comparing and analyzing the results of pore water pressure consolidation of piles under different drainage schemes, the design principles for surface storage of CFT were determined.

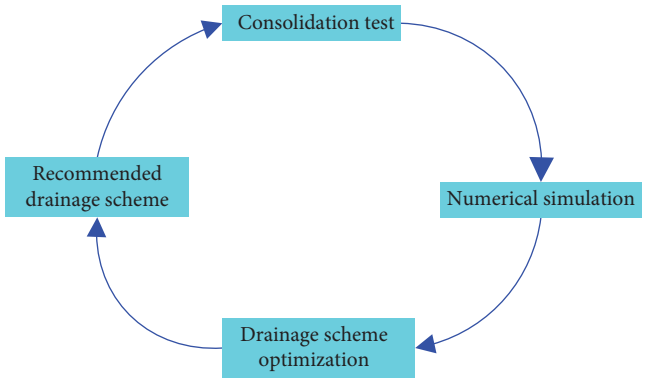

Figure 1: The technical route of this study.

Figure 2: The fully automatic pneumatic consolidation instrument.

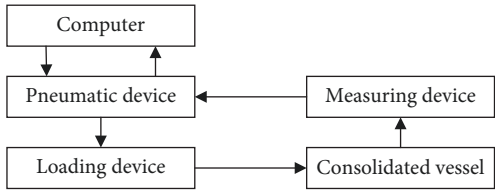

Figure 3: The schematic diagram of the automatic pneumatic consolidation instrument.

2. Experimental Study of Consolidation Characteristics

In order to study the deformation characteristics of the CFT in the consolidation process after storage, the consolidation test of the original tailings and the CFT at different ages was carried out in this study. The test was carried out using a fully automatic pneumatic consolidation instrument, and the photographs of the instrument are shown in Figure 2.

The automatic pneumatic consolidation instrument mainly consists of a consolidation vessel, a loading device, a measuring device, a pneumatic device, and a computer control system, so the test process is controlled automatically and data are collected by a computer system. The schematic diagram of the automatic pneumatic consolidation instrument can be seen in Figure 3. The main technical parameters of the deformation measuring device are as follows:

(i) The range of the dial indicator is 10 mm and the index value is 0.01 mm;

(ii) The maximum allowable error is ±0.2% F.S.

Table 1 lists the mix ratio of the CFT. Each cubic meter of the mix includes 4.97 kg of flyash, 2.26 kg of CaO, 0.72 kg of cement, 0.36 kg of plaster, and 0.72 kg of fiber. Figure 4 shows the details of raw material pictures, mixed and homogenized according to the ratios in Table 1, and the finished mixture of CFT is shown in Figure 5.

The height of the accumulation body in actual engineering is about 18 m and the unit weight of the CFT is about 18.6 kN/m^3, so the maximum principal stress of this structure is not exceeding $18\,\text{m} \times 18.6\,\text{kN/m}^3 = 334.8\,\text{kPa}$, so loadings of 12.5, 25, 50, 100, 200, and 400 kpa are adopted to simulate the stress state of the structure.

The test process is as follows: weigh the material according to the optimal ratio, mix it well and leave it to stand; take samples. Place the ring knife upside down on a small glass plate with a soil mixing knife to fill the ring knife with CFT, exclude air bubbles and scrape flat, weighing; place the guard ring, permeable plate, and thin filter paper in the consolidation container, carefully place the specimen with the ring knife into the guard ring, then place the thin filter paper, permeable plate, and pressurized cover plate on the specimen, place it under the pressurized frame, align the pressurized frame right in the middle, and install the gauge; the specimens with age requirements were cured in the ring knife at 0, 3, and 7 days intervals, the curing method refers to curing the specimen at the room temperature $20° \pm 2°$ and relative humidity above 95% RH, of which no curing was required for the 0 day age-CFT; set all levels of pressure, the consolidation process is divided into six levels of loading, respectively, 12.5, 25, 50, 100, 200, and 400 kpa; the first five levels of each level of time are 2 hr, the judgment of the last level of loading stability conditions is 0.005 mm, and record the test data; clear the displacement to zero, click start test to realize the automatic loading and judgment of stability of the consolidation test, and end the test automatically when the test end conditions are met. The consolidation test loading and curing specimens are shown in detail in Figure 6. For the pure tailings, the consolidation test was performed directly after cutting the pure tailings with a cutting ring.

The pore ratio after consolidation and stabilization at each pressure level is calculated by the following equation:

$$e_i = e_0 - (1 + e_0)\frac{\sum \Delta h_i}{h_0}, \tag{1}$$

where e_i is the pore ratio at a certain level of pressure; $\sum \Delta h_i$ is the total deformation of the height of the specimen at a certain level of pressure, cm; h_0 is the initial height of the specimen, cm.

Based on the test results of axial deformation of the specimens under each level of loading, the e–p curves and e–lgp curves of the CFT specimens were obtained by calculating in accordance with Equation (1) and are shown in detail in Figure 7. The former is a downwardly concave curve, and

Table 1: Mix ratio for the consolidation test of CFT.

SN	Tailings slurry concentration	Aggregate–cement ratio	Tailings	Curing material (kg/kg)					Water
				Flyash	CaO	Cement	Plaster	Fiber	
1	74%	20	180.8	4.97	2.26	0.72	0.36	0.72	66.7

Figure 4: Raw materials of the CFT.

Figure 5: The mixed evenly CFT.

the latter is an upwardly convex curve.*e–lgp* curves generally show a tendency to be flatter at low pressures and to steepen with increasing pressure. As the curing age increases, the initial section of the*e–p* curve decreases to a greater extent, which is related to the participation of water in the hydration reaction of CFT and evaporation, free flow, and thus the increase of porosity ratio. Under the first step loading, this part of the pore space is rapidly compressed, which is manifested in the *e–p* curve as a rapid decline of the initial section, and the degree of decline is positively correlated with the age of curing.

The compression coefficient under side-limiting conditions is the slope of the cut line of the *e–p* curve: $a_v = -\frac{\Delta e}{\Delta p}$. The volume compression modulus is $m_v = \frac{a}{1+e_0}$, where e_0 is the initial porosity.

The variation process of compression coefficient a_v and compression modulus m_v of CFT with loading at different ages is shown in detail in Figure 8. The compression modulus represents the ratio of the body strain increment to the effective pressure increment of the CFT. According to the test results, the compression modulus value is the largest between the first and second stage loads, and with the application of the third stage load, the compression modulus shows a steep decreasing trend; with the gradual increase of load, the compression modulus gradually tends to zero. The results of compression coefficient a_v fitting show that the greater the age, the greater the value of compression coefficient in general, the compression coefficient and vertical pressure show a power function relationship, the exponent of the power function is close to 1 (0.988–0.99), and the coefficient before the power function is negative (−17.43 to −6.45). As the age increases, the overall compression modulus value is larger, and the compression modulus m_v shows a power function relationship with the vertical pressure, with the exponent of the power function being negative (−0.51 to −5.57) and the advance coefficient of the power function being positive.

3. Research on the Method of Pile Consolidation and Drainage

In order to study the pore water pressure relief process in the pile with/without interlayer drains, two schemes were designed to carry out the consolidation simulation of CFT. The free-drainage boundary conditions for Scheme 1 are the surfaces on both sides of the pile and the bottom of the pile; i.e., the pore water inside the pile is free to seep outward through the seepage pipes on the surfaces and at the bottom under the effect of hydraulic gradient and infiltration. The drainage boundary conditions of Scheme 2 not only contain the surface drainage and bottom drainage of Scheme 1 but also add interlayer drains in the middle of the first layer, the

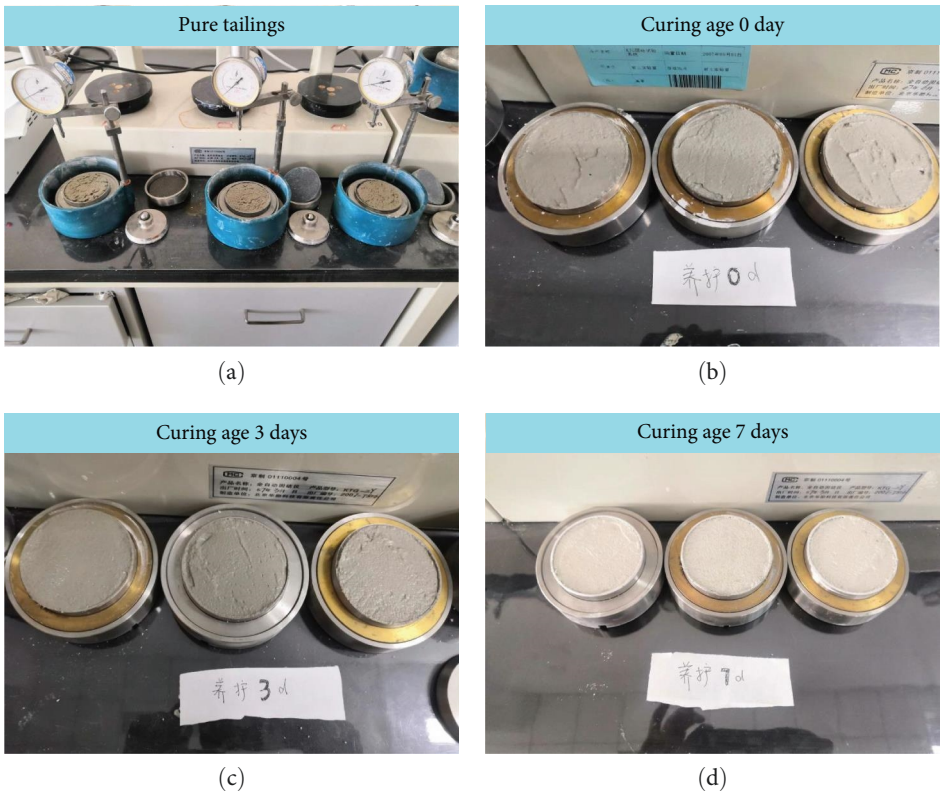

Figure 6: Pure tailings (a); curing age 0 day (b); curing age 3 days (c); curing age 7 days (d).

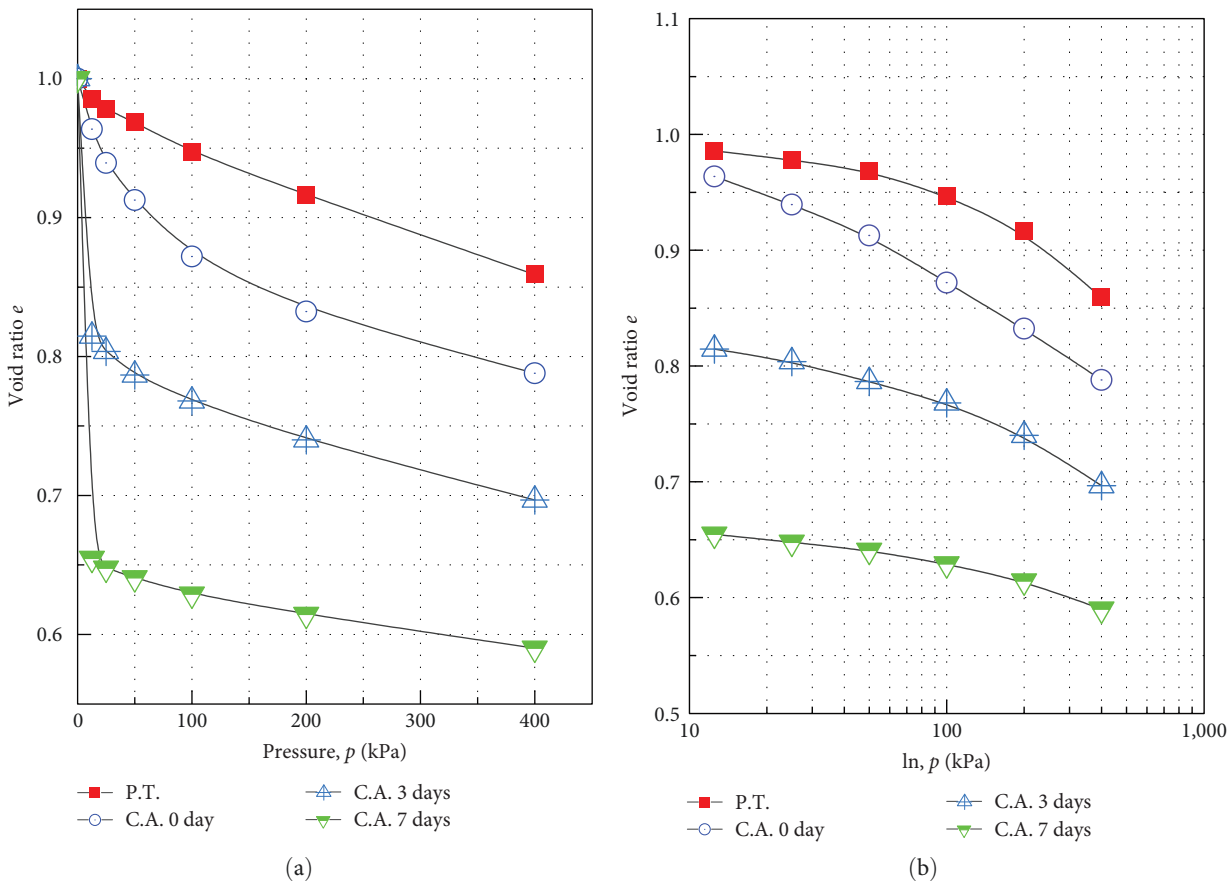

Figure 7: Axial deformation curves of the CFT specimens: (a) e–p curve; (b) e–$lg\ p$ curve.

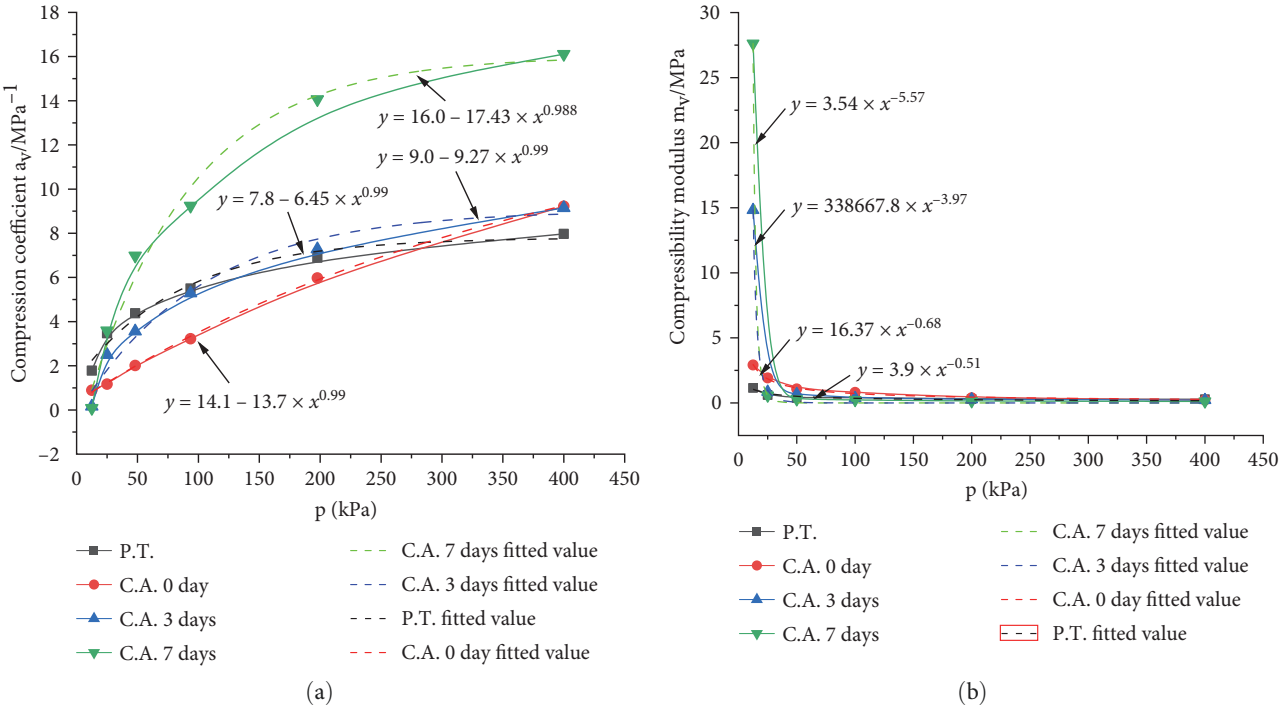

Figure 8: The variation process of compression coefficient (a) and compression modulus (b) with loading at different ages.

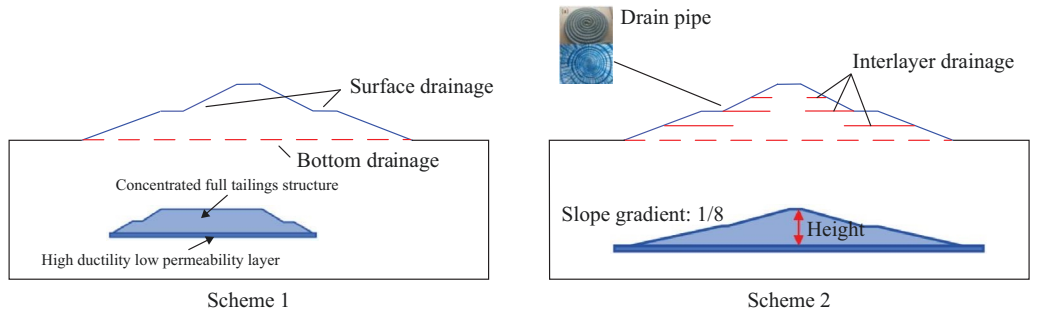

Figure 9: The schematic diagrams of the schematic diagrams of CFT pile.

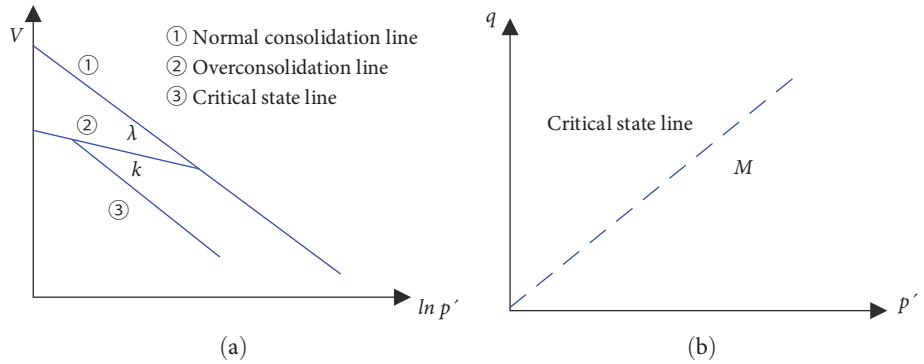

Figure 10: Modified cambridge model: (a) pressure–volume relationship; (b) critical state line.

demarcation position between the first layer and the second layer, and the middle of the second layer to enhance the drainage effect inside the pile. The schematic diagrams of surface drainage, bottom drainage, and interlayer drainage scheme are shown in Figure 9.

Due to the addition of curing materials within the CFT to enhance its cohesion value, its properties are similar to those of clay materials. Therefore, in this study, with reference to clay materials, the modified Cam–Clay detailed in Figure 10 is used to simulate the consolidation process of the CFT material.

Table 2: The parameters of the CFT for consolidation simulation.

No.	Material	Unit weight (kN/m^3)	Saturated weight (kN/m^3)	Poisson's ratio	Permeability coefficient (m/d)	Initial void ratio	Overconsolidation ratio	Normal consolidation line slope	Overconsolidation line slope	Critical state line slope
1	CFT	18.5	19.0	0.38	0.00864	1.0	0.5	1.217	0.013	1.217
2	Foundation	20.0	21	0.3	0.000864	—	—	—	—	—

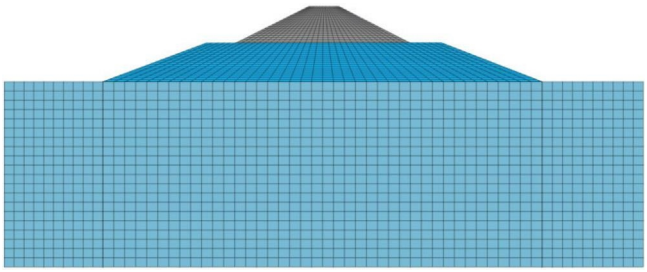

Figure 11: The finite element model for consolidation calculation.

Where κ is the overconsolidation line slope, λ is the normal consolidation line slope, and M is the critical state line slope. The normal consolidation line slope λ and the overconsolidation line slope κ are estimated as follows:

$$\lambda = \frac{C_c}{2.303}, \quad \kappa = \frac{C_s}{2.303}, \tag{2}$$

where C_c is the compression index, $C_c = -\Delta e/\Delta(\ln p)$ is the slope of the straight line segment in the $e - \ln p$ curve, and C_s is the resilience index or recompression index, which is obtained from the $e - \ln p$ curve of the one-dimensional consolidation test, $C_s \ll C_c$, for the general clay $C_s \approx (1/10 \sim 1/5)C_c$.

The slope M of the critical state line is estimated from the effective internal friction angle (the angle of internal friction obtained in the drainage test):

$$M = \frac{6 \sin \phi}{3 - \sin \phi}, \tag{3}$$

where ϕ is the angle of internal friction obtained in the triaxial compression test.

Referring to the consolidation test curves, the consolidation analysis parameters of the CFT pile are detailed as shown in Table 2. The model is divided into two components, the pile body and the foundation, where the CFT pile is modeled using the modified Cam–Clay and the foundation is modeled using the Mohr–Coulomb model.

The finite element model for consolidation calculation established according to the design drawing of the pile body is shown in detail in Figure 11, with a total of 2,600 divided units and 2,721 nodes. The horizontal simulation range is 1,650 m, and the vertical simulation range is 670 m, including 190 m for the pile and 480 m for the foundation.

When considering the continuity for mass in a tiny volume, the amount of water flowing out of the tiny volume is compared to the mass concentration changes by the same amount. Pore pressure is used as a variable in seepage analysis, which can be obtained by Darcy's law expressed in terms of pore pressure governing equations for seepage analysis:

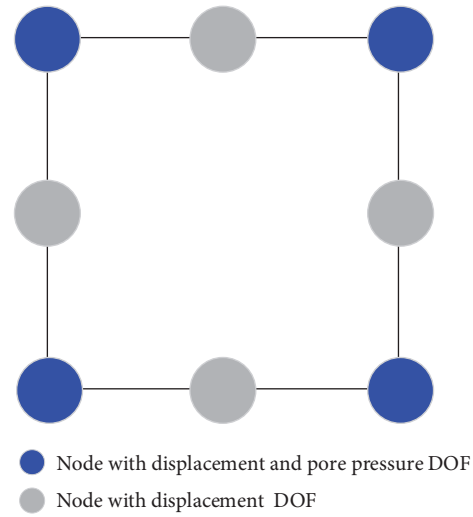

Figure 12: Degree of freedom of high-order continuous consolidation element.

$$\frac{1}{\gamma_w}\nabla^T(k\nabla p) - \nabla^T\left(kn_g\right) = \left(\frac{nS}{\rho_w}\frac{\partial \rho_w}{\partial p} + n\frac{\partial S}{\partial p}\right)\frac{\partial p}{\partial t}, \tag{4}$$

where γ_w is the volume weight of water, kN/m^3; p is the hydraulic pressure, m^2/s; k is the permeability coefficient matrix, m/d; n_g is the unit vector in the direction of gravity; n is the void ratio; S is the degree of saturation.

High-order continuous consolidation elements are adopted in this study, as is shown in Figure 12.

According to the above scheme to establish the consolidation analysis finite element calculation model, the total length of the calculation 180 days, the calculation of the step length of 3 days, that is, a total of 60 time steps, and the obtained results of the internal pore water pressure change process of Scheme 1 and Scheme 2 in each typical time step are shown in Figures 13 and 14.

According to the cloud diagram of pore water pressure calculation, it can be seen that under the scheme without interlayer drainage facilities, the large value of pore water pressure is concentrated in the center to the top of the pile, and the negative pore water pressure area is concentrated in the left and right side of the pile in the first layer of the first step, which is a symmetrical distribution of left and right characteristics. The distribution of the pore water pressure cloud diagram in the whole section is uniform, and the change is continuous. In Scheme 2, due to the installation of the interlayer drainage pipe, the pore water pressure distribution cloud diagram in the pore pressure concentration area and the location of the extreme value have been effectively dispersed, which is different from the continuous change of the whole cross-section presented by the pore water pressure cloud diagram without the drainage pipe. It is shown that the installation of interlayer drainage pipes accelerates the evacuation of pore water within the piles around them, so that the pore water pressure cloud is

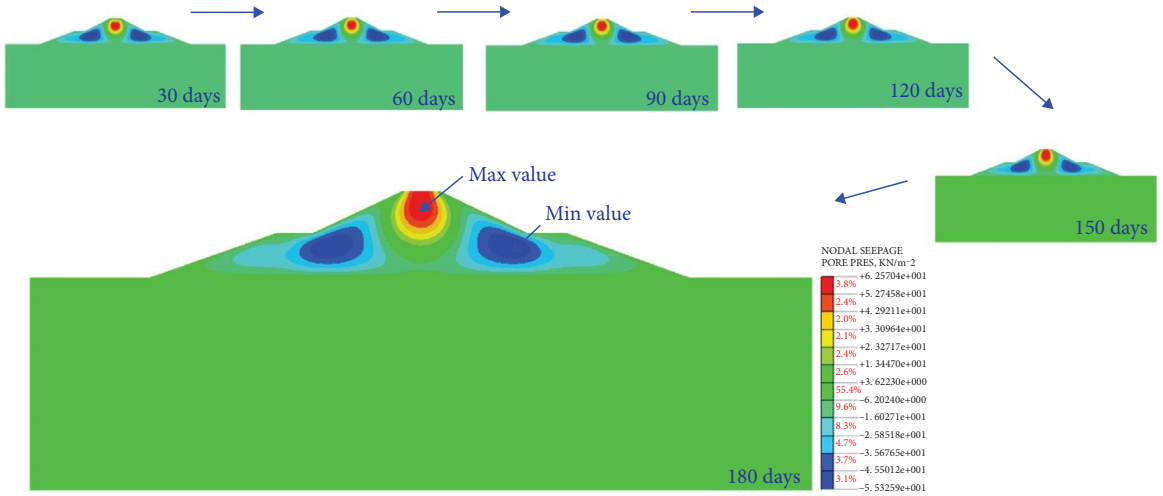

Figure 13: Cloud diagram of pore water pressure calculation in scheme 1.

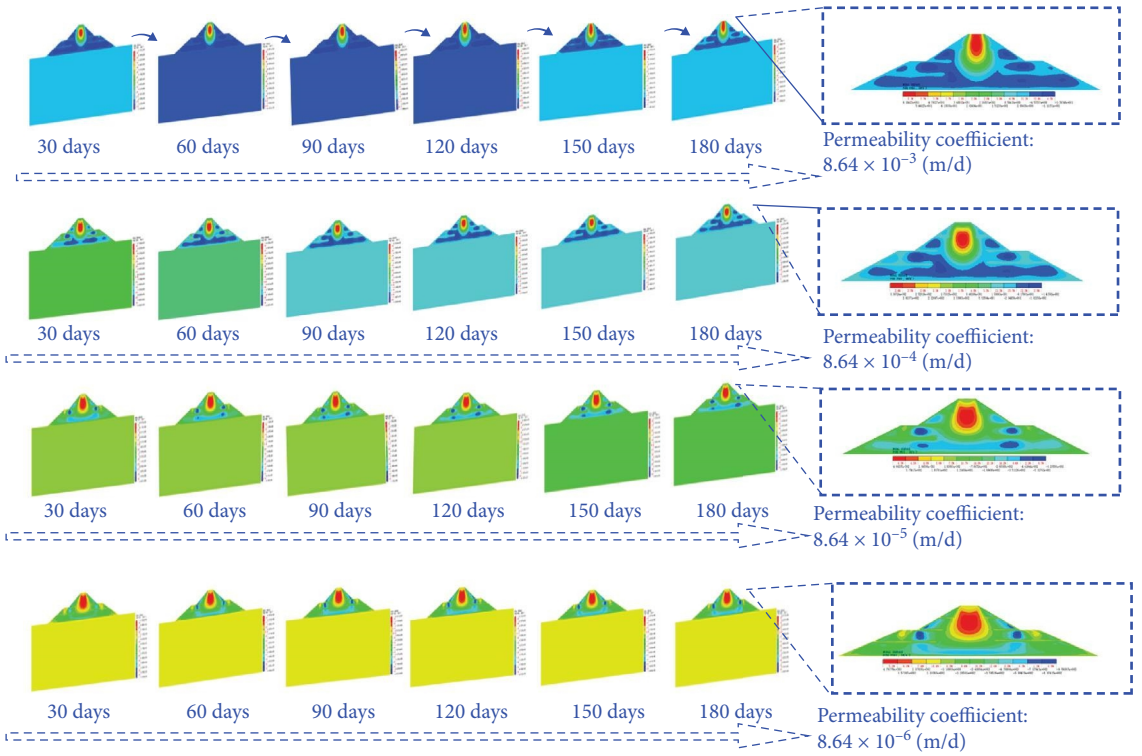

Figure 14: Cloud diagram of pore water pressure calculation in scheme 2.

interrupted at the drainage pipes and locally concentrated between the two layers of drainage pipes.

The extreme results of finite element calculation of pore water pressure in the pile with different permeability coefficients are shown in detail in Figure 15. Based on the calculation results, it can be seen that compared with no interlayer drainage facilities, when the interlayer drainage facilities are set up, the very small value of the whole cross-section is reduced, and the very large value is increased, but the increase is not obvious when the permeability coefficient is 8.64×10^{-3} m/d. As the permeability coefficient of the pile decreased (changing from 8.64×10^{-3} to 8.64×10^{-6} m/d), the magnitude of the change in the pore pressure extremes across the full cross-section of the pile increased compared to the absence of interlayer drainage facilities. As the permeability coefficient decreases, the negative pore water pressure extremes gradually decrease and the positive pore water pressure extremes gradually increase, indicating that the degree of pore pressure accumulation increases with the decrease of the permeability coefficient. Therefore, the necessity of interlayer drainage is greater when the permeability of the concentrated tailings is poor.

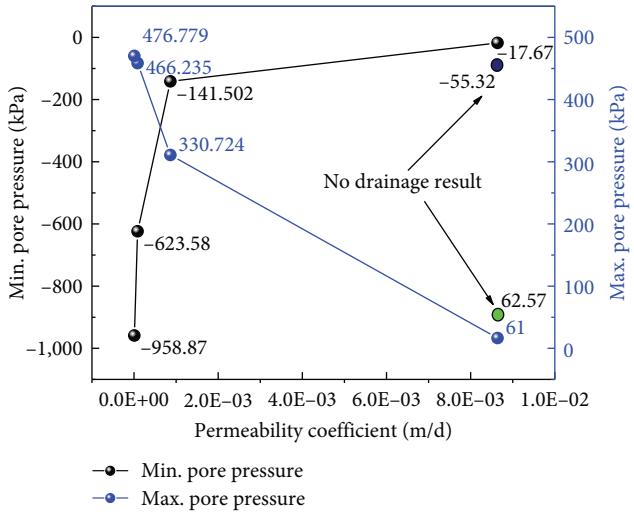

FIGURE 15: The extreme results of pore water pressure in the pile with different permeability coefficients.

In order to quantitatively analyze the change rule of pore water pressure with time at different points inside the pile under different drainage schemes, and to compare the effect of pore water pressure relief inside the concentrated tailings pile with different permeability coefficients, five nodes, namely, 3755, 3859, 4340, 3110, and 4362, were selected in the computational model of the study (see Figure 14 for details). We extracted the pore water pressure results of each calculation step and plotted the pore water pressure versus time curves of different permeability coefficient schemes without internal interlayer drainage and with drainage schemes, and the obtained process lines of pore water pressure change at each node are detailed as shown in Figure 16.

Based on the calculation results, it can be seen that, in general, the pore water pressure at the study points inside the pile (node 3755 and node 3110) is overall positive, and the pore water pressure at the study points at the edge of the pile (node 3859 and node 4362) is overall negative. The study point at the bottom of the pile (node 4340), although located inside the pile, also shows a negative pore water pressure due to the strong drainage facilities at the bottom.

Analyzing from the trend of pore water pressure change with time, when the permeability coefficient is 8.64×10^{-3} m/d, the process line of pore water pressure at each study point with and without interlayer drainage basically overlaps. Therefore, it is not obvious that setting up interlayer drainage has an effect on relieving pore water inside the pile when the permeability coefficient is large, and it is recommended that no interlayer drainage be set up when the permeability coefficient is greater than 8.64×10^{-3} m/d; the drainage effect can be achieved by relying on the surface drainage and the bottom drainage only. As the permeability coefficient decreases (changing from 8.64×10^{-3} to 8.64×10^{-6} m/d), the pore water pressure at the same point in time at node 3755 of the study site (Figure 16(a)) gradually rises, and the lower the permeability coefficient, the more pronounced is the tendency for unsteady seepage (the curve continues to rise) at the end of the computation ($t = 180$ days). Taking $k = 8.64 \times 10^{-6}$ m/d as an example, the slope of the nodal pore water pressure process line at $t = 180$ days is still high, and the pore water pressure still shows a relatively fast upward trend, indicating that the reduction of the permeability coefficient affects the pore water pressure relief process in the center part of the pile. Therefore, it is recommended that the project should take appropriate drainage measures in conjunction with the permeability coefficient of the pile. When the permeability coefficient is low, the number of interlayer drainage facilities should be increased to accelerate the evacuation of pore water inside the pile.

The upper surface study point of the pile, node 3859 (Figure 16(b)), and the lower surface study point, node 4362 (Figure 16(e)), have negative pore water pressures because they are near the surface of the pile. When the permeability coefficient $k \geq 8.64 \times 10^{-4}$ m/d, the pore pressure curve will converge regionally at a specific time point; i.e., the variation of pore pressure with time tends to be close to 0. When the permeability coefficients $k = 8.64 \times 10^{-5}$ and $k = 8.64 \times 10^{-6}$ m/d, the pore pressure curves still show a decreasing trend at $t = 180$ days and do not reach the convergence point. The results of pore water pressure calculations for different permeability coefficients at the bottom center of the pile at node 4340 (Figure 16(c)) are basically similar to those at the surface nodes 3859 (Figure 16(b)) and 4362 (Figure 16(e)), with a slight difference in the quantitative values. Therefore, the research results show that the smooth and efficient drainage facilities at the bottom of the pile can effectively reduce the pore pressure of the concentrated tailings in its lower part, prevent the situation of excess pore water pressure, and maximize the consolidation effect of the pile.

According to the calculation results, it can be seen that the pore water pressure calculation results of the scheme with interlayer drainage pipe are lower than that of the scheme without drainage pipes, indicating that the scheme with drainage pipes can effectively reduce the excess pore water pressure inside the pile. Therefore, it is recommended that in the actual project, a drain pipe through to the surface should be installed inside the pile to accelerate the drainage of the pore water inside the CFT and then accelerate the consolidation process of the pile.

4. Conclusions

In this study, to address the problem that the high water content of the CFT is unfavorable for on-site storage and strength growth, we carried out a consolidation test study and a coupled seepage–stress field analysis and obtained the following conclusions:

(1) The results of consolidation tests at different ages show that the larger the age, the larger the overall value of the compression coefficient, and the compression coefficient and vertical pressure show a power function increasing law; the larger the age, the larger the compression modulus value overall,

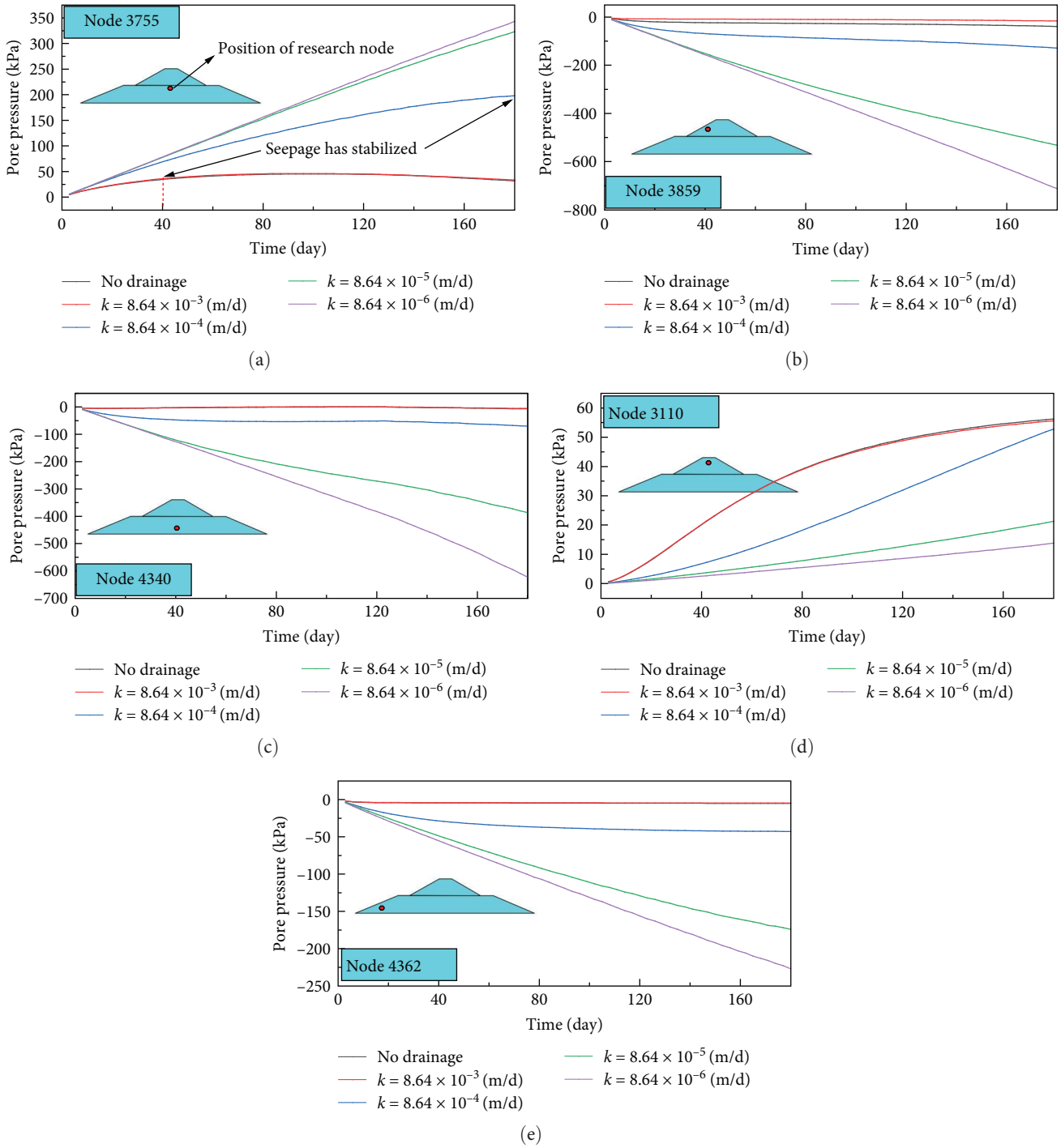

FIGURE 16: Pore water pressure relief process with different permeability coefficients: node 3755 (a); node 3859 (b); node 4340 (c); node 3110 (d); node 4362 (e).

and the compression modulus shows a power function decreasing relationship with the vertical pressure; in general, the value of consolidation deformation of CFT with added curing material is larger than that of pure tailings, and there is a big difference between the consolidation characteristics of the pure tailings and that of the pure tailings.

(2) Numerical simulation results of the full cross-section consolidation of the CFT pile show that the results of the pore water pressure in the cross-section under the surface drainage only and bottom drainage scheme are higher than those of the scheme containing interlayer drainage. Upon completion of consolidation, the pore water pressure cloud diagrams of the latter showed the characteristics of fragmented aggregation and discontinuity at the drains, indicating that the solution with interlayer drains was superior to the solution without interlayer drains.

(3) As the permeability coefficient of the concentrated tailings body increases, the pore water pressure at the study point inside the pile gradually increases, and the phenomenon of internal pore pressure accumulation becomes serious; the pore water pressure curve at the end of the simulation has a lower tendency to converge. Therefore, it is recommended that before the design of the internal structure of the pile, full consideration should be given to the permeability characteristics of the pile material and ultimately to design drainage facilities that match the permeability parameters of the pile.

Data Availability

The data used to support the findings of this study are available from the corresponding author upon request.

Conflicts of Interest

The authors declare that the research was conducted in the absence of any commercial or financial relationships that could be construed as a potential conflict of interest.

Authors' Contributions

Guodong Mei was responsible for conceptualization, project administration, and funding acquisition. Sha Wang was responsible for methodology, formal analysis, investigation, original draft preparation, and visualization. Lijie Guo was responsible for validation, writing, reviewing, and editing, and supervision. Sha Wang and Yali Wang were responsible for resources. Sha Wang and Yifan Chu were responsible for data curation. All the authors have read and agreed to the published version of the manuscript.

Acknowledgments

This research was funded by the National Key Research and Development Plan of China (grant number 2023YFC3012204) and the National Natural Science Foundation Project of China (grant number 52274122). The APC was funded by the Exploration Fund of BGRIMM Technology Group (grant number 02-2271) and the National Key Research and Development Plan of China (grant number 2018YFC0604605).

References

[1] S. Wang, C. Zhang, W. Zhu, F. Wang, and W. Cao, "Influence of solidified tailing concentration on initial fluidity and strength," *Metal Mine*, vol. 2, pp. 136–138, 145, 2008.

[2] S. Liu, Y. Sun, G. Li, G. Liu, Z. Qi, and F. Wang, "Analysis on the early strength of backfill with unclassified tailings in a gold mine," *Mining R & D*, vol. 40, no. 3, pp. 125–129, 2020.

[3] J. Zhang, G. Che, and W. Zhang, "Variation of shear strength parameters of iron tailings with the degree of consolidation," *China Earthquake Engineering Journal*, vol. 43, no. 2, pp. 453–458, 2021.

[4] Y. Cui, G. Mei, B. Chang, and Y. Wang, "Mechanical properties of modified solidification tailings," *Nonferrous Metals (Mining Section)*, vol. 72, no. 3, pp. 93–98,112, 2020.

[5] W.-B. Xu, W.-L. Wu, and B. Liu, "Effect of curing age, cement content and confining pressure on the saturated hydraulic conductivity and triaxial compressive behavior of cemented tailings backfill," *Journal of Central South University*, vol. 30, pp. 1649–1661, 2023.

[6] S.-M. Chen, E. Yilmaz, Z.-G. Xiang, and Y.-M. Wang, "Curing conditions effect on pore structure, compressive strength and elastic modulus of cementitious tailings backfills," *Powder Technology*, vol. 422, Article ID 118458, 2023.

[7] O. Benkirane, S. Haruna, and M. Fall, "Strength and microstructure of cemented paste backfill modified with nano-silica particles and cured under non-isothermal conditions," *Powder Technology*, vol. 419, Article ID 118311, 2023.

[8] Y. Fan, C. Wang, X. Liu, X. Wang, and M. Jiang, "Experimental study on strength evolution of filling body under curing with stress," *Mining R & D*, vol. 42, no. 3, pp. 83–88, 2022.

[9] E. Yilmaz, T. Belem, B. Bussière, M. Mbonimpa, and M. Benzaazoua, "Curing time effect on consolidation behaviour of cemented paste backfill containing different cement types and contents," *Construction and Building Materials*, vol. 75, pp. 99–111, 2015.

[10] X. Qin, P. Wang, L. Liu, M. Wang, and J. Xin, "Sensitivity analysis of microstructure parameters and mechanical strength during consolidation of cemented paste backfill," *Mathematical Problems in Engineering*, vol. 2018, Article ID 5170721, 9 pages, 2018.

[11] K. Li, "*Study on mechanical and acoustic emission characteristics of uniaxial compression of cemented tailings backfill subjected to temperature*," M.S. thesis, Wuhan University of Science and Technology, Wuhan, 2019.

[12] X. Ke, "*Study on structure and properties of the consolidation mass of cemented tailings backfill*," Ph.D. thesis, Wuhan University, Wuhan, 2016.

[13] D. Deng, F. Liu, Z. Yao et al., "Investigation on properties of cement -tailing backfill under conventional triaxial compression," *Mining R & D*, vol. 31, no. 3, pp. 15-16, 54, 2011.

[14] K. Zhao, Y. Zhou, Q. Huang et al., "Early properties and modeling of cemented superfine tailings backfill containing sodium dodecyl sulfate: microstructure, mechanics, and acoustics," *Mechanics of Materials*, vol. 179, Article ID 104567, 2023.

[15] S. Yin, J. Liu, J. Shao, H. Zhang, B. Armelle, and Y. Kou, "Influence rule of early compressive strength and solidification mechanism of full tailings paste with coarse aggregate," *Journal of Central South University (Science and Technology)*, vol. 51, no. 2, pp. 478–488, 2020.

[16] W. Li and M. Fall, "Strength and self-desiccation of slag-cemented paste backfill at early ages: link to initial sulphate concentration," *Cement and Concrete Composites*, vol. 89, pp. 160–168, 2018.

[17] Q. Ma, G. Liu, X. Yang, and L. Guo, "Physical model investigation on effects of drainage condition and cement addition on consolidation behavior of tailings slurry within backfilled stopes," *International Journal of Minerals, Metallurgy and Materials*, vol. 30, pp. 1490–1501, 2023.

[18] K. Fang and L. Cui, "Experimental investigation of evolutive mode-I and mode-II fracture behavior of fiber-reinforced cemented paste backfill: effect of curing temperature and curing time," *Frontiers of Structural and Civil Engineering*, vol. 17, pp. 256–270, 2023.

[19] W. Xu, Q. Li, and M. Tian, "Strength and deformation properties of polypropylene fiber-reinforced cementedtailings backfill," *Chinese Journal of Engineering*, vol. 41, no. 12, pp. 1618–1626, 2019.
[20] K. Zhao, C. Ma, J. Yang et al., "Pore fractal characteristics of fiber-reinforced backfill based on nuclear magnetic resonance," *Powder Technology*, vol. 426, Article ID 118678, 2023.
[21] Y. Liu, B. Zhan, Y. Yu, J. Li, Y. Zhou, and Q. Yu, "Preparation and strength mechanism of slag-based mine backfill for low concentration ultra-fine tailings," *Construction and Building Materials*, vol. 384, Article ID 131457, 2023.
[22] S. Wang, C. Zhang, W. Zhu, F. Wang, W. Cao, and J. Miu, "Influence of soldifying additive on the initial flidity and strength of soldified tailings," *Metal Mine*, vol. 2, pp. 30–33,86, 2009.
[23] Q. Dong, "*Study of evolution and mechanism of the strength to sulfur content Lead-Zinc tailings cemented paste backfill*," DPh. D. thesis, Liaoning Technical University, 2017.
[24] B. Wang, S. Gan, and P. Dong, "Experimental study on consolidation characteristics of tailings cemented backfill in alpine regions," *The Chinese Journal of Nonferrous Metals*, vol. 32, no. 8, pp. 2446–2457, 2022.
[25] Y. Hou, S. Cao, P. Ding, X. Zhang, and D. Han, "Effect of freeze-thaw cycle on the intensity of consolidated full tailings," *Metal Mine*, vol. 7, no. 1, pp. 34–39, 2019.
[26] Y. Zou, Y. Yang, and X. Zhang, "Experimental study and analysis on variation characteristics of mechanical parameters of tailings filled material under cyclic loading and unloading," *Value Engineering*, vol. 39, no. 11, pp. 276–280, 2020.
[27] G. Zhao, D. Su, Y. Zhang, and W. Wu, "Study on creep test of cemented tailings backfill and statistical damage model," *Metal Mine*, vol. 5, pp. 26–30, (in Chinese), 2016.
[28] J. Li, "*The experimental research of creep characteristic and long- term strength for cemented full tailings backfill*," M.S. thesis, Jiangxi University of Science and Technology, 2018.
[29] W. Wang, G. Cao, Y. Li et al., "Experimental study of dynamic characteristics of tailings with different reconsolidation degrees after liquefaction," *Frontiers in Earth Science*, vol. 10, Article ID 876401, 2022.
[30] G. Cao, W. Wang, G. Yin, and Z. Wei, "Experimental study of shear wave velocity in unsaturated tailings soil with variant grain size distribution," *Construction and Building Materials*, vol. 228, Article ID 116744, 2019.
[31] M. Ito and S. Azam, "Large-strain consolidation modeling of mine waste tailings," *Environmental Systems Research*, vol. 2, Article ID 7, 2013.
[32] L. Cui and M. Fall, "Multiphysics model for consolidation behavior of cemented paste backfill," *International Journal of Geomechanics*, vol. 17, no. 3, Article ID 04016077, 2017.
[33] M. Shahsavari and M. Grabinsky, "Pore water pressure variations in cemented paste backfilled stopes," in *Geo-Chicago 2016*, pp. 331–342, ASCE, 2016.
[34] B. Erçikdi, F. Cihangir, A. Kesimal, H. Deveci, and İ. Alp, "Effect of drainage conditions on the strength of paste backfill," *Scientific Mining Journal*, vol. 47, no. 2, pp. 15–24, 2008.